

MICROBIOLOGY

Silver Enhances Antibiotic Activity Against Gram-Negative Bacteria

Jose Ruben Morones-Ramirez,^{1,2,*†} Jonathan A. Winkler,^{1,3,*} Catherine S. Spina,^{2,4} James J. Collins^{1,2,3,4‡}

A declining pipeline of clinically useful antibiotics has made it imperative to develop more effective antimicrobial therapies, particularly against difficult-to-treat Gram-negative pathogens. Silver has been used as an antimicrobial since antiquity, yet its mechanism of action remains unclear. We show that silver disrupts multiple bacterial cellular processes, including disulfide bond formation, metabolism, and iron homeostasis. These changes lead to increased production of reactive oxygen species and increased membrane permeability of Gram-negative bacteria that can potentiate the activity of a broad range of antibiotics against Gram-negative bacteria in different metabolic states, as well as restore antibiotic susceptibility to a resistant bacterial strain. We show both in vitro and in a mouse model of urinary tract infection that the ability of silver to induce oxidative stress can be harnessed to potentiate antibiotic activity. Additionally, we demonstrate in vitro and in two different mouse models of peritonitis that silver sensitizes Gram-negative bacteria to the Gram-positive-specific antibiotic vancomycin, thereby expanding the antibacterial spectrum of this drug. Finally, we used silver and antibiotic combinations in vitro to eradicate bacterial persister cells, and show both in vitro and in a mouse biofilm infection model that silver can enhance antibacterial action against bacteria that produce biofilms. This work shows that silver can be used to enhance the action of existing antibiotics against Gram-negative bacteria, thus strengthening the antibiotic arsenal for fighting bacterial infections.

INTRODUCTION

There is a growing need to enhance our antibacterial arsenal, given the rising incidence of antibiotic resistance and the emergence of new virulent pathogens (1, 2). This is particularly true for infections caused by Gram-negative bacteria, which are difficult to treat because these organisms have a protective outer membrane consisting of lipopolysaccharides (3). Drug-resistant, Gram-negative bacterial infections have forced clinicians to revisit the use of older antimicrobials that have previously been discarded (2, 4, 5). Silver is intriguing because its antimicrobial properties were first documented around 400 B.C. when Hippocrates described its use to enhance wound healing and preserve water and food (6). Despite this long-standing history and its demonstrated activity against Gram-negative bacteria, the complete bactericidal mode of action of silver remains unclear (7–15). Here, we use a systems-based approach to identify the mechanistic effects of silver on Gram-negative bacteria. We then harness these mechanisms to potentiate and expand the activity of existing antibiotics.

RESULTS

Ag⁺ induces OH• production and increases membrane permeability

We used ionic silver (Ag⁺) in a silver nitrate salt (AgNO₃) and found substantial antimicrobial activity (~3 log) at 30 μM against log-phase growing *Escherichia coli*, a model Gram-negative bacterium (Fig. 1A

and table S1). Production of reactive oxygen species (ROS), such as hydroxyl radicals (OH•), may be a common mechanism of cell death induced by bactericidal antibiotics (16–21), although the role of ROS in antibiotic-induced bacterial killing is a matter of debate (22, 23). We measured hydroxyl radicals in untreated *E. coli* cells and in cells treated with Ag⁺ for 1 hour using 3'-(*p*-hydroxyphenyl) fluorescein (HPF) dye (24). Ag⁺-treated cells exhibited detectable increases in fluorescence compared to untreated cells, indicating increased OH• production (Fig. 1B). Moreover, reducing ROS through the addition of thiourea, a ROS scavenger (25) (fig. S1A), or by overexpressing superoxide dismutase (*sodA*) (fig. S1B) inhibited Ag⁺-induced bacterial cell death, confirming that ROS production may be critical for the observed bactericidal activity.

Hydroxyl radicals are a product of Fenton chemistry, where free iron plays a key role (26). We measured the effect of Ag⁺ on iron homeostasis by using an engineered promoter *E. coli* strain that produces the GFP in response to Fur, a master regulator of iron metabolism (21). After 1 hour of Ag⁺ treatment, the reporter strain exhibited increased fluorescence relative to untreated cells (fig. S2A), indicating a disruption in iron concentrations within the cell. We then studied the effect of Ag⁺ on two mutant *E. coli* strains with impaired iron regulation: a Δ *tonB* strain, which has a blocked exogenous iron uptake system (27), and a Δ *discS* strain, which exhibits a smaller number of internal Fe-S clusters (28). Δ *tonB* had similar sensitivity to Ag⁺ as the wild-type strain, whereas Δ *discS* exhibited a bacteriostatic phenotype when subjected to Ag⁺ treatment (Fig. 1C). Δ *discS* also exhibited significantly lower OH• production ($P < 0.001$) in response to Ag⁺ treatment compared to the treated wild-type cells (fig. S2B). These results suggest that internal iron from Fe-S clusters plays a role in Ag⁺-mediated cell death.

Transition metals, such as silver, copper, and zinc, can break down or inactivate Fe-S clusters (29, 30) and cause leakage of Fe²⁺. We therefore tested the ability of silver to disrupt Fe-S clusters and cause release of Fe²⁺ by measuring Fe²⁺ concentrations using Ferene-S, a colorimetric dye (31), in an Ag⁺-treated *E. coli* cell lysate. We compared the

¹Howard Hughes Medical Institute, Department of Biomedical Engineering and Center of Synthetic Biology, Boston University, Boston, MA 02215, USA. ²Wyss Institute for Biologically Inspired Engineering, Harvard University, Boston, MA 02118, USA. ³Program in Molecular Biology, Cell Biology, and Biochemistry, Boston University, Boston, MA 02215, USA. ⁴Boston University School of Medicine, 715 Albany Street, Boston, MA 02118, USA. *These authors contributed equally to this work.

[†]Present address: Universidad Autónoma de Nuevo León, UANL, Facultad de Ciencias Químicas, Av. Universidad S/N, Cd. Universitaria, San Nicolás de los Garza, N.L. 66450, México.

[‡]Corresponding author. E-mail: jcollins@bu.edu

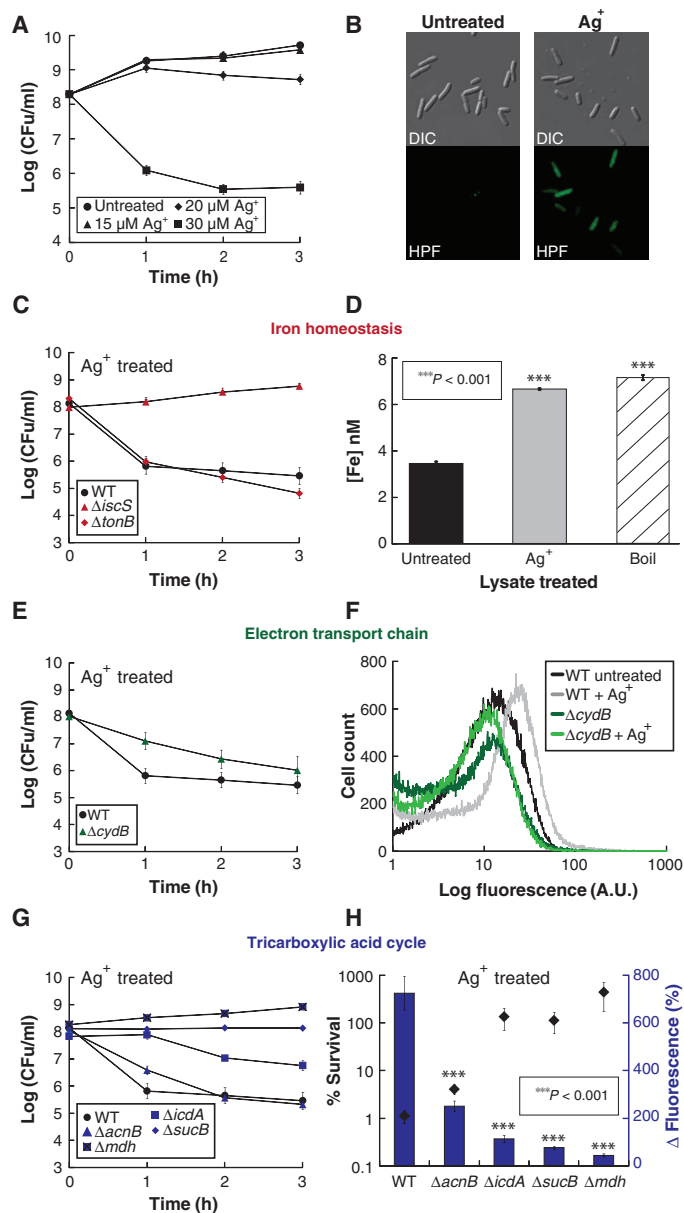


Fig. 1. Ag^+ induces $\text{OH}\cdot$ production through a metabolic cascade and iron misregulation. (A) Kill curves for log-phase growing wild-type (*WT*) *E. coli* treated with various concentrations of AgNO_3 . (B) Bright-field and fluorescence microscopy of HPF-stained untreated *E. coli* cells and cells treated with 30 μM AgNO_3 after 1 hour. (C) Survival of iron homeostasis gene knockout mutants relative to WT when treated with 30 μM AgNO_3 . (D) Free iron [Fe^{2+}] concentration in a cell lysate after 1 hour of treatment with heat (90°C) or 30 μM AgNO_3 . (E) Survival of an electron transport gene knockout mutant relative to WT when treated with 30 μM AgNO_3 . (F) GFP fluorescence histogram from the *soxS* reporter, incorporated into a WT and ΔcydB strain of *E. coli*, after 1 hour of treatment with 30 μM AgNO_3 . (G) Survival of tricarboxylic acid (TCA) cycle gene knockout mutants relative to WT when treated with 30 μM AgNO_3 . (H) Blue bars show percent change in fluorescence for HPF (hydroxyl radical production), HPF-stained WT, and TCA cycle mutant strains of *E. coli* treated for 1 hour with 30 μM AgNO_3 relative to the HPF-stained untreated strains. The diamond data points represent percent survival after 1 hour of treatment with 30 μM AgNO_3 . Error bars represent means \pm SEM from at least three biological replicates. *** $P < 0.001$, Student's *t* test, significant difference from the untreated lysate in (D) and the treated WT in (H).

absorbance to a positive control, a cell lysate heated to 90°C to disrupt Fe-S clusters, and a negative control, an untreated lysate. Ag^+ -treated lysates showed significantly higher Fe^{2+} concentrations relative to the untreated lysate ($P < 0.001$) (Fig. 1D), demonstrating that Ag^+ directly interacts with and disrupts Fe-S clusters. Because stress-induced superoxide disrupts Fe-S clusters (21), we measured the response of a *soxS* reporter strain, which expresses GFP upon activation of SoxR by superoxide, to Ag^+ treatment and found that Ag^+ does indeed induce superoxide production (fig. S3). This result suggests that Ag^+ also indirectly leads to Fe^{2+} leakage by stimulating the production of superoxide. Together, these findings indicate that Ag^+ disturbs internal iron homeostasis by directly and indirectly disrupting intracellular Fe-S clusters.

Superoxide is formed as a by-product of electron transfer through the electron transport chain (ETC) (32). The ETC component cytochrome bd-I oxidase has been shown to be crucial for superoxide production under conditions of stress (33). We therefore explored whether cytochrome bd is one of the sources of Ag^+ -mediated superoxide production. We found that a cytochrome bd knockout strain (ΔcydB) was 10 times less sensitive to a 1-hour Ag^+ treatment than wild type (Fig. 1E) and exhibited ~ 3 times lower concentrations of superoxide in response to the treatment (Fig. 1F), indicating that cytochrome bd is a source of Ag^+ -mediated superoxide production.

We also explored the role of the TCA cycle, a metabolic pathway that feeds the ETC, in Ag^+ -induced cell death. We examined cell viability and $\text{OH}\cdot$ production in Ag^+ -treated TCA cycle gene knockout strains (ΔicdA , ΔsucB , Δmdh , ΔacnB) and observed that all the knockout strains were less sensitive to Ag^+ treatment than wild type (Fig. 1G). Additionally, there was a distinct correlation between the Ag^+ -induced percent change in $\text{OH}\cdot$ production in the mutant strains and their susceptibility to Ag^+ (Fig. 1H), indicating that a functional TCA cycle facilitates Ag^+ -mediated $\text{OH}\cdot$ production. These findings show that Ag^+ disrupts metabolic pathways that drive Fenton chemistry and lead to the overproduction of $\text{OH}\cdot$ and cell death.

We next used transmission electron microscopy (TEM) to explore the physical changes that occur to bacterial cells as a result of Ag^+ treatment (Fig. 2A and fig. S4, A to C). Ag^+ treatment at bactericidal concentrations caused protein aggregation, indicated by the high-density aggregates observed within the *E. coli* (9) and drastic morphological changes in the cell envelope. We reasoned that the observed Ag^+ -induced physical alterations in cell morphology could be indicative of an overall increase in outer membrane permeability. To explore this, we used propidium iodide (PI), a membrane-impermeable fluorescent dye that has been used to detect permeation of the cell membrane (see Supplementary Materials and Methods and fig. S5). Ag^+ -treated cells showed increased PI fluorescence relative to untreated cells, indicating destabilization of the cellular envelope and increased membrane permeability (Fig. 2B).

The protein aggregates observed in the TEM images of Ag^+ -treated cells suggest the occurrence of protein misfolding. Ag^+ is capable of strongly interacting in vitro with sulfhydryl ($-\text{SH}$) groups found in a variety of proteins (34). These functional groups form disulfide bonds in many proteins, which contribute to their overall shape, functionality, and stability. We hypothesized that Ag^+ disrupts disulfide bond formation in vivo, which would contribute to protein misfolding and aggregation. To monitor disulfide bond formation during Ag^+ treatment, we used a *dps* reporter strain (fig. S6) that expresses GFP when the protein OxyR forms a disulfide bond in the presence of H_2O_2 (35). We

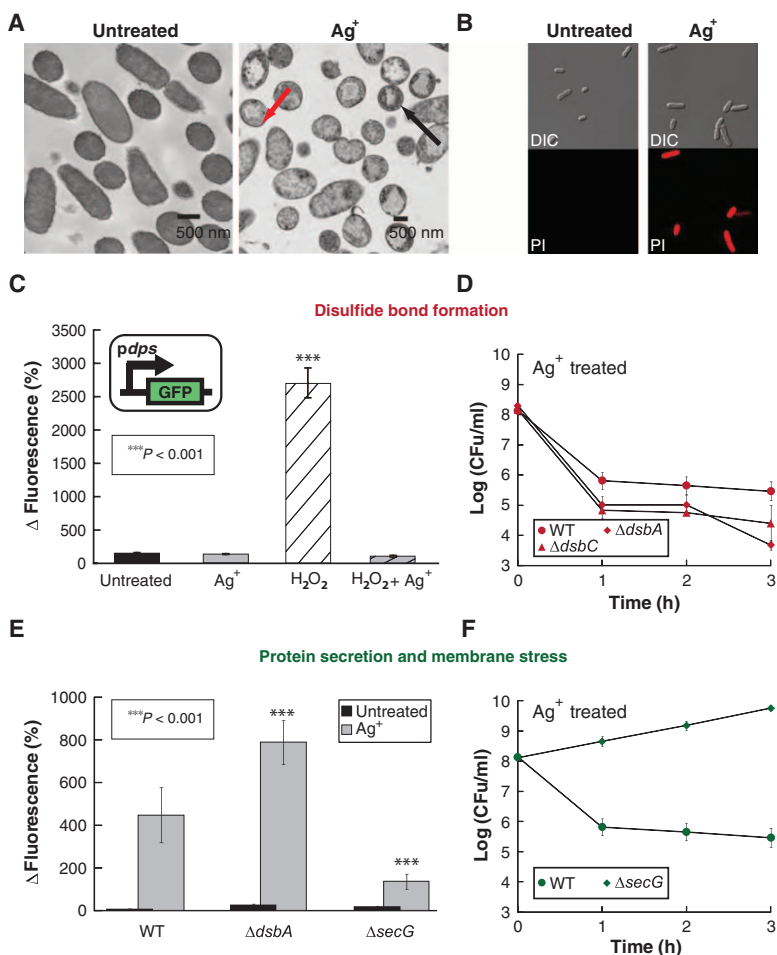


Fig. 2. Ag⁺ increases membrane permeability through disruption of disulfide bond formation and misfolded protein secretion. (A) TEM micrographs showing untreated (left) and 30 μM AgNO₃-treated *E. coli*. The red arrow indicates a cell showing outer membrane separation, which is indicative of membrane stress. The black arrow indicates a cell exhibiting protein aggregation (9). (B) Bright-field and fluorescence microscopy of PI-stained untreated cells and cells treated for 1 hour with 30 μM AgNO₃. (C) Change in green fluorescent protein (GFP) fluorescence from the disulfide bond genetic reporter strain after 1 hour of the following treatments: 30 μM AgNO₃, 0.5 mM H₂O₂, and the combination of both. Values shown are relative to fluorescence at time zero before treatment. (Inset) Schematic of the reporter strain, which is based on activation of the *dps* promoter. (D) Survival of disulfide bond formation gene knockout mutants relative to WT when treated with 30 μM AgNO₃. (E) Change in fluorescence of PI (membrane permeability), PI-stained WT, Δ*dsbA*, and Δ*secE* strains of *E. coli* after 1 hour of treatment with 30 μM AgNO₃. (F) Survival of protein secretion gene knockout mutants relative to WT when treated with 30 μM AgNO₃. Error bars represent means ± SEM from at least three biological replicates. ****P* < 0.001, Student's *t* test, significant difference from the untreated control in (C) and the treated WT in (E).

treated the reporter strain with H₂O₂, Ag⁺, and a combination of both (Fig. 2C). As expected, cells treated with H₂O₂ showed increased fluorescence relative to untreated cells. The addition of Ag⁺ to the H₂O₂ treatments reduced the fluorescence back to untreated levels, indicating that Ag⁺ is capable of inhibiting or disrupting protein disulfide bond formation in vivo.

We next explored whether disrupting protein disulfide bond formation can affect membrane permeability. Disulfide bond formation

is mediated by DsbA, a disulfide oxidoreductase. We found that an untreated Δ*dsbA* strain was more permeable than an untreated wild-type strain (fig. S7), indicating that impairment of disulfide bond formation is sufficient for increasing permeability. Furthermore, we tested the effect of Ag⁺ on the Δ*dsbA* strain because it exhibits a higher frequency of proteins with exposed sulfhydryl groups (36), and found that it was more sensitive (Fig. 2D) and more permeable (Fig. 2E) than the Ag⁺-treated wild-type strain. Knocking out DsbC, the enzyme responsible for disulfide bond repair, resulted in a phenotype similar to that exhibited by Δ*dsbA* (Fig. 2D).

Ag⁺-induced misfolded proteins that are secreted from the cytoplasm and transported to the outer membrane could lead to the observed membrane destabilization and increased permeability (37). We evaluated the effect of Ag⁺ on a Δ*secE* strain, which exhibits an impaired protein translocation machinery (38), and found that it was less permeable (Fig. 2E) and less susceptible to Ag⁺ treatment (Fig. 2F) compared to wild type. These results indicate that the translocation of misfolded proteins contributes to Ag⁺-mediated cellular membrane permeability.

These findings indicate that Ag⁺ targets and disrupts multiple cellular processes, including disulfide bond formation, central metabolism, and iron homeostasis, and that these changes are associated with increases in ROS production and bacterial membrane permeability.

Ag⁺ potentiates bactericidal antibiotics both in vitro and in vivo

We next explored the possibility of using Ag⁺ as an antibiotic adjuvant, harnessing different mechanistic features of its mode of action. We first reasoned that the capacity of Ag⁺ to disrupt metabolic processes and iron homeostasis would enable it to potentiate bactericidal antibiotics that share a common mechanism of action involving the overproduction of ROS (17). We treated *E. coli* with low, sublethal concentrations of gentamicin (an aminoglycoside antibiotic), ampicillin (a β-lactam antibiotic), and ofloxacin (a quinolone antibiotic) (table S1). When we added sublethal concentrations of Ag⁺ to these antibiotic treatments, we observed significantly enhanced antimicrobial activity (*P* < 0.001) (Fig. 3A, fig. S8, A to C, and table S3). We used the Bliss Model to determine the nature of the therapeutic effects exhibited by the drug combinations (39, 40). We quantified the degree of synergy at 1 and 3 hours between Ag⁺ and each of the individual antibiotics and found their interactions to be synergistic for all cases (fig. S9). We also measured OH• in the treated cells and observed no detectable increases in ROS production resulting from the sublethal antibiotic treatments (Fig. 3B). However, the addition of sublethal doses of Ag⁺ to the antibiotic treatments induced marked increases in ROS, suggesting that Ag⁺ can prime cells for ROS production (*P* < 0.001) (Fig. 3B). Together, these results indicate that the ability of Ag⁺ to stimulate Fenton chemistry can be harnessed to potentiate the activity of antibiotics that use ROS as part of their bactericidal mechanism.

We also examined whether the ability of Ag⁺ to increase membrane permeability could be exploited to enhance the intracellular influx of antibiotics. We first tested if Ag⁺-mediated cell membrane

permeability could be used to restore drug sensitivity to bacterial strains that have developed resistance through activation of efflux pumps and decreased antibiotic permeation. To test this possibility, we used an *E. coli* strain (AG112) that contains a mutation in the *marR* gene, which renders the strain resistant to multiple antibiotics, including the bacteriostatic drug tetracycline (41). We found that AG112 exhibits a threefold higher tetracycline minimum inhibitory concentration (MIC) than does the wild-type (AG110) *E. coli* strain (Fig. 3E and

table S4). Treating AG112 with a sub-inhibitory concentration of Ag⁺ (15 μM) in combination with tetracycline restored the resistant strain's tetracycline MIC to wild-type levels (Fig. 3E). These data show that Ag⁺ can enhance the antibiotic susceptibility of drug-resistant cells, potentially by increasing membrane permeability to the antibiotic.

As noted earlier, infections caused by Gram-negative bacteria are often difficult to treat (2). These bacteria have a protective outer membrane that prevents the entry of a variety of larger antibiotics, such as the glycopeptide vancomycin (3). We reasoned that the ability of Ag⁺ to increase outer membrane permeability could be used to render vancomycin active against Gram-negative bacteria, thereby broadening the antibacterial spectrum and clinical utility of this antibiotic. We treated *E. coli* with low doses of Ag⁺ and vancomycin individually and in combination, and found that the combination treatments resulted in significantly greater ($P < 0.001$) bacterial cell death relative to treatments with Ag⁺ or vancomycin alone (Fig. 3C, fig. S10, A to C, and table S5). Using the Bliss Model, we determined the antimicrobial effects between Ag⁺ and vancomycin to be synergistic at all of the concentrations tested (fig. S11). Moreover, the increased cell death we observed correlated with increases in membrane permeability resulting from the addition of Ag⁺ (Fig. 3D). These results indicate that Ag⁺ can be combined with vancomycin to form a drug combination that harnesses Ag⁺-induced outer membrane permeability changes to enable vancomycin to become effective against Gram-negative bacteria.

We next examined whether the doses of Ag⁺ used in this study have a toxic effect on mammalian systems. We first assessed Ag⁺ toxicity in vitro using an MTT [3-(4,5-dimethylthiazol-2-yl)-2,5-diphenyltetrazolium bromide] cell viability assay on different human primary cells and cell lines. Our results showed that the cells exhibited no change in viability upon direct exposure to the Ag⁺ concentrations used in this work (Fig. 4A). Although Ag⁺ is currently approved by the U.S. Food and Drug Administration (FDA) as a topical antimicrobial (42), we investigated the possibility of using Ag⁺ as an adjuvant in combination therapies through other delivery routes (that is, intraperitoneally). Ag⁺ toxicity delivered intraperitoneally was measured in vivo by determining the median lethal dose (LD₅₀), which is the drug dose at which 50% of the treated mice survive (Fig. 4B). We determined an LD₅₀ between 120 and 240 μM, a result that is consistent with those of earlier toxicity studies (43). A standard way to establish the safety and efficiency of a drug is through the therapeutic index (ratio between LD₅₀ and therapeutic concentrations) (44, 45). On the basis of our results, we calculated a therapeutic index for Ag⁺ that ranges from 8 to 16, an index that is well within the ranges of the therapeutic indices reported for FDA-approved antibiotics, such as vancomycin (44), tobramycin, gentamicin, colistin, and polymyxin B (45).

We next evaluated the effects of Ag⁺ on the blood chemistry and organ function of healthy, infection-free mice 6, 24, and 48 hours after treatment by measuring key metabolite and enzyme concentrations using the Piccolo Comprehensive Metabolic Reagent Disk from Abaxis (fig. S12, A and B). Mice treated with Ag⁺ showed normal kidney and pancreatic function, as well as normal concentrations of ions and trace metals (fig. S13, A to D). We observed increased concentrations of the hepatic enzymes alkaline phosphatase and alanine aminotransferase (fig. S13B) at the initiation of treatment; however, the mice stabilized and recovered to concentrations within the normal range 48 hours after treatment (fig. S14, A and B). Elevated hepatic enzyme concentrations have been considered safe if they are reversible and not accompanied by increases in total bilirubin (46). Total bilirubin concentrations

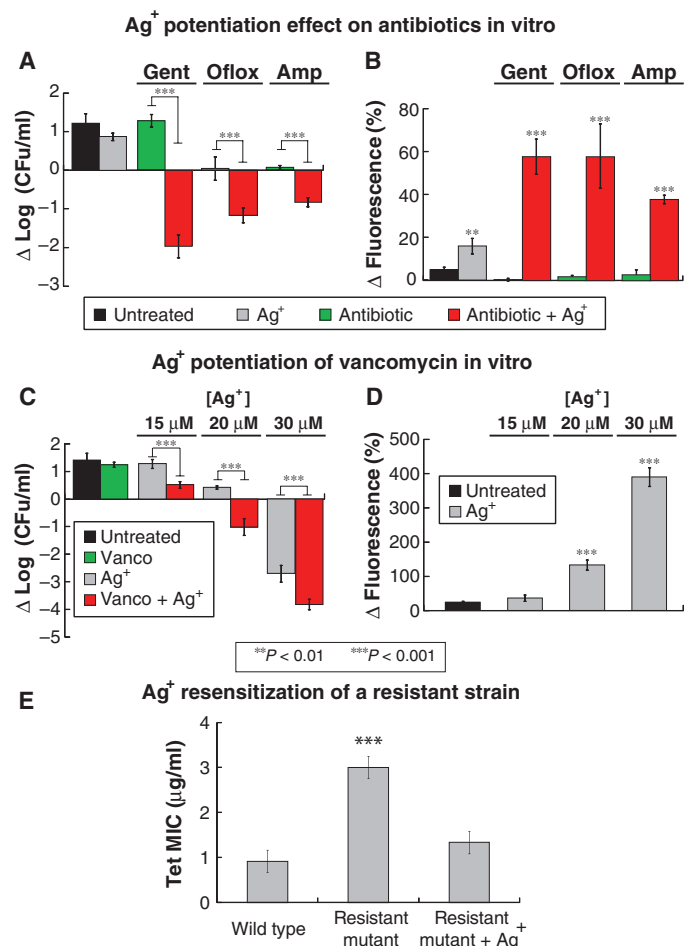


Fig. 3. Ag⁺ potentiates bactericidal antibiotics in vitro. (A) Log change in colony-forming units (CFU)/ml, from time zero, of WT *E. coli* after treatment for 3 hours with 15 μM AgNO₃, gentamicin (Gent) (0.25 μg/ml), ofloxacin (Oflox) (0.03 μg/ml), ampicillin (Amp) (1 μg/ml), and combinations of AgNO₃ with the respective antibiotics. (B) Changes in HPF fluorescence after 1 hour of administering the treatments described in (A). (C) Log change in CFU/ml, from time zero, of WT *E. coli* after treatment for 3 hours with the indicated concentrations of AgNO₃ and vancomycin (30 μg/ml). (D) Changes in PI fluorescence after 1 hour of administering different concentrations of AgNO₃. Error bars represent means ± SEM from at least six biological replicates. Ten mice per treatment group were used for the survival studies. (E) Treatment of a drug-resistant *E. coli* strain with Ag⁺ restores antibiotic susceptibility back to WT levels. Tetracycline MIC of WT *E. coli* (AG110) and that of an *E. coli* drug-resistant strain (AG112) with and without Ag⁺ treatment. *** $P < 0.001$, ** $P < 0.05$, Student's *t* test, significant difference from the WT strain or untreated control, unless otherwise specified. Error bars represent means ± SEM from at least three biological replicates.

remained within normal limits throughout the Ag^+ treatments (fig. S13B). Although further studies are needed to determine the toxicity of Ag^+ , these in vivo results suggest that the Ag^+ dosages used in this study are well tolerated by mice.

We used a mouse model of acute peritonitis to examine whether the mechanistic effects of Ag^+ observed in vitro (increased membrane permeability and $\text{OH}\cdot$ production) are also observed in vivo after Ag^+ treatment (Fig. 5A). One hour after inoculation of the bacteria into the peritoneal cavity, the mice were treated with either phosphate-buffered saline (PBS) or $30\ \mu\text{M}$ Ag^+ delivered intraperitoneally. One hour after treatment, the bacteria within the peritoneal cavity were collected and tested for $\text{OH}\cdot$ production and increased permeability using HPF and PI dyes, respectively (Fig. 5B). Treating mice with Ag^+ increased both HPF (Fig. 5C) and PI (Fig. 5D) fluorescence of the bacteria in the intraperitoneal cavity, demonstrating that Ag^+ treatment increases hydroxyl radical production and bacterial cell wall permeability in vivo (Fig. 5). On the basis of these results, we hypothesized that low doses of Ag^+ may potentiate antibiotic activity in vivo.

We first examined whether Ag^+ could potentiate gentamicin activity in vivo by testing the effects of Ag^+ and gentamicin individually and in combination on a mouse urinary tract infection (UTI) model. UTI infections are one of the most commonly occurring infections in clinical settings (47). The infection was established in the bladder through transurethral catheterization and delivery of 2×10^9 MG1655 *E. coli* cells suspended in an aqueous solution containing mucin (Fig. 6A). Twenty-four hours after infection, the mice received no treatment or intraperitoneally administered gentamicin, Ag^+ , or gentamicin plus Ag^+ . Treatment with gentamicin or Ag^+ alone resulted in no effect on bladder *E. coli* cell counts 24 hours after treatment related to the control, whereas treatment with gentamicin plus Ag^+ reduced the cell counts by fourfold (Fig. 6, B and C). These results demonstrate that Ag^+ is capable of potentiating antibiotic activity in vivo.

We also examined whether Ag^+ could potentiate vancomycin activity in vivo. We analyzed the effects of Ag^+ and vancomycin individually and in combination in mouse models of acute and mild peritonitis. The infection was established in the peritoneal cavity through intraperitoneal injection of either 1×10^4 MG1655 *E. coli* cells (mild model) (Fig. 7A) or 5×10^6 MG1655 *E. coli* cells (acute model) (Fig. 7C), suspended in an aqueous solution containing mucin. One hour (for acute infection model) and 24 hours (for mild infection model) after infection, the mice received either no treatment or intraperitoneal delivery of vancomycin, Ag^+ , or vancomycin plus Ag^+ . We monitored two aspects of the infection: the *E. coli* cell counts within the peritoneal cavity (in

both models) and mouse survival (only for the acute peritonitis model because the mild infection model was not lethal). In the mild peritonitis model, the combination of Ag^+ plus vancomycin led to a significant cell count reduction relative to the control (Fig. 7B). In the acute model, we observed that treatment with vancomycin or Ag^+ alone resulted in no effect on intraperitoneal *E. coli* cell counts after 24 hours, whereas treatment with vancomycin plus Ag^+ reduced the cell counts by 100-fold (Fig. 7D). Additionally, in the acute intraperitoneal model, 90% of mice treated with the vancomycin plus Ag^+ combination survived

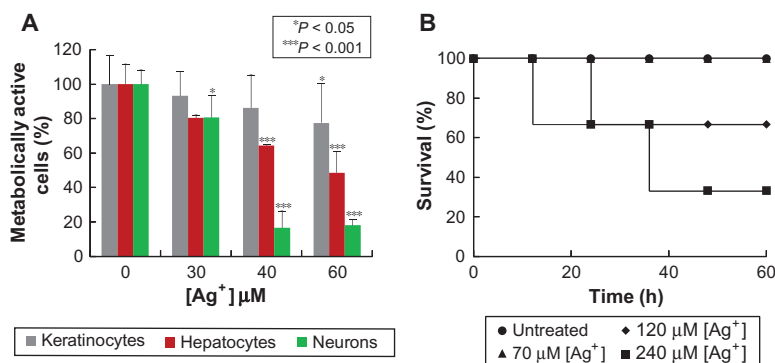


Fig. 4. Toxicity studies of Ag^+ showing that low levels of Ag^+ are not cytotoxic. (A) Percentage of metabolically active human cell lines (keratinocytes, hepatocytes, and neurons) after being treated with increasing Ag^+ concentrations. (B) Survival of mice treated with the following: no treatment and 70, 120, and 240 μM AgNO_3 . Survival studies were done using 10 mice per group. *** $P < 0.001$, * $P < 0.05$, Student's *t* test, significant difference from the untreated control. Error bars represent means \pm SEM from at least three biological replicates.

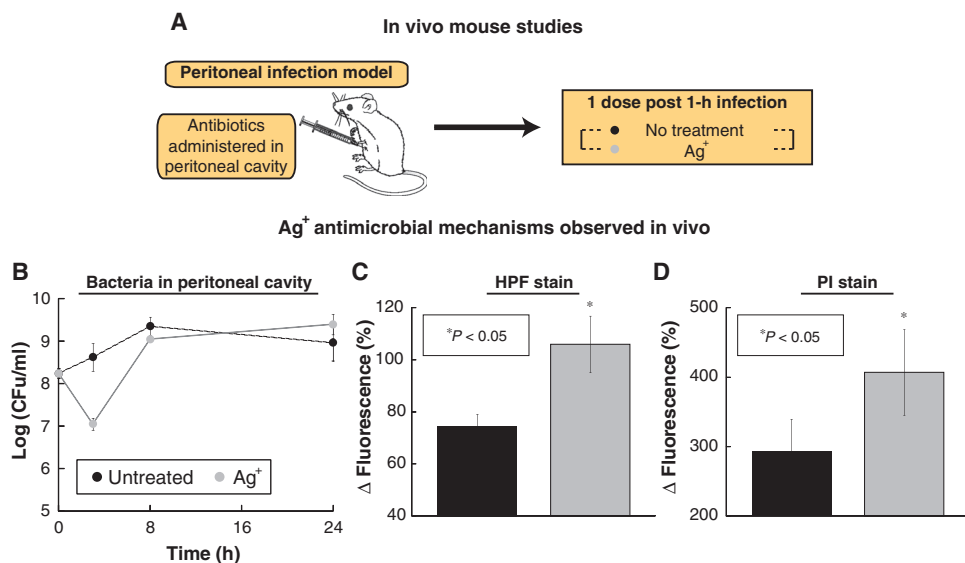


Fig. 5. Mode of action of Ag^+ in in vivo mild and acute peritonitis models. (A) Schematic of the in vivo animal experiments. (B) Bacterial counts in peritoneal cavity for experiment showing in vivo Ag^+ bactericidal mechanism of action. Kill curves of WT *E. coli* within the peritoneal cavity of mice after no treatment and treatment with AgNO_3 (6 mg/kg) (35 μM). (C and D) Change in fluorescence of the HPF-stained (C) and PI-stained (D) *E. coli* cells harvested from the peritoneal cavity of mice that developed a peritoneal infection for 3 hours and were treated 1 hour after (4 hours total after infection) with AgNO_3 (6 mg/kg) (35 μM). Error bars represent means \pm SEM from at least 10 biological replicates. * $P < 0.05$, Student's *t* test, significant difference from the untreated control.

Fig. 6. Ag⁺ potentiates bactericidal antibiotic activity in vivo in a UTI mouse model.

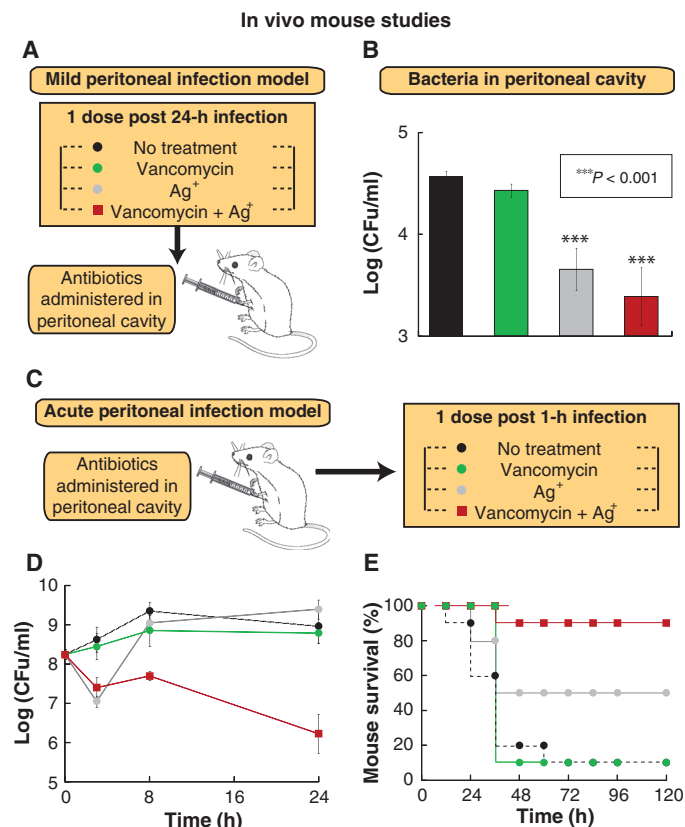
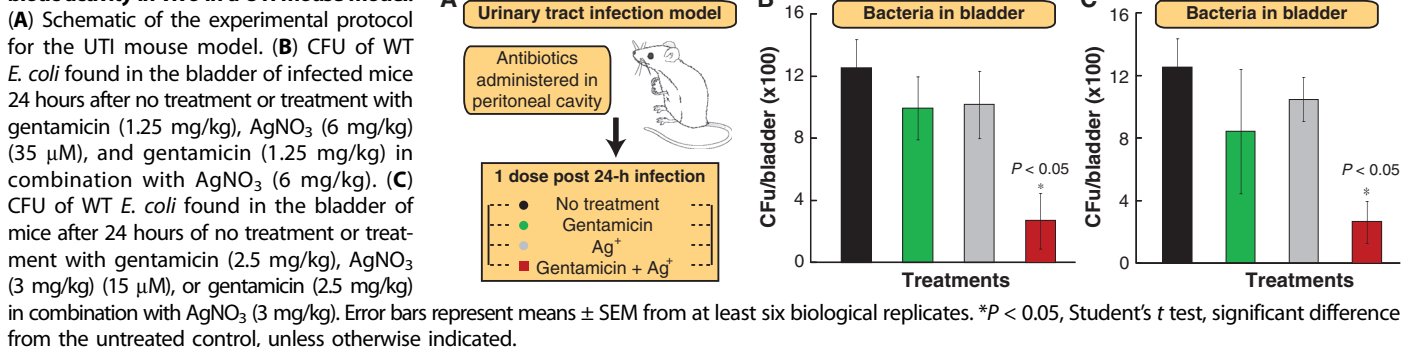


Fig. 7. Ag⁺ potentiates vancomycin activity in a mouse peritonitis infection model.

(A) Schematic of the experimental protocol for the mild peritonitis mouse model. (B) Kill curves of WT *E. coli* within the peritoneal cavity of mice after no treatment or treatment with vancomycin (30 mg/kg), AgNO₃ (6 mg/kg) (35 μM), and vancomycin (30 mg/kg) in combination with AgNO₃ (6 mg/kg). (C) Schematic of the experimental protocol for the mouse model of acute peritonitis. (D) Kill curves of WT *E. coli* within the peritoneal cavity of mice after no treatment or treatment with vancomycin (30 mg/kg), AgNO₃ (6 mg/kg) (35 μM), or vancomycin (30 mg/kg) in combination with AgNO₃ (6 mg/kg). (E) Survival of mice with an acute intra-peritoneal infection induced with an initial inoculum of 5 × 10⁶ WT *E. coli* after no treatment or treatment with vancomycin (30 mg/kg), AgNO₃ (6 mg/kg) (35 μM), or vancomycin (30 mg/kg) in combination with AgNO₃ (6 mg/kg). Error bars represent means ± SEM from at least six biological replicates. ***P < 0.001, Student's *t* test, significant difference from the untreated control. Ten mice per treatment group were used for the survival studies.

(after 5 days), compared with 50% of mice treated with Ag⁺ alone and 10% of mice treated with vancomycin alone or just the vehicle (Fig. 7E). These findings demonstrate the possibility of using Ag⁺ to enhance the activity of vancomycin against Gram-negative pathogens in vivo.

Ag⁺ potentiates bactericidal antibiotics against bacterial persisters and biofilms

Bacterial persisters, which are dormant cells within an isogenic bacterial population that are tolerant to antibiotic treatment, are thought to play an important role in chronic recurring infections and the formation of biofilms. Both of these represent an important economic burden for the health care industry because they directly contribute to increased hospital visits from patients with deteriorating health conditions. This has stimulated research to find viable ways to treat and eliminate bacterial persisters (48, 49). We explored the effect of Ag⁺ on bacterial persisters in vitro. We treated *E. coli* persister cells with a range of Ag⁺ concentrations and found increased antimicrobial activity above 60 μM (Fig. 8A). We next measured HPF and PI fluorescence in untreated persister cells and cells treated for 3 hours with lethal (60 μM) and sublethal (30 μM) Ag⁺ concentrations. Ag⁺-treated cells showed increases in both HPF (Fig. 8B) and PI (Fig. 8C) fluorescence compared to untreated bacterial persisters. These results, in combination with data noted above, provide evidence that Ag⁺ treatment drives increased production of ROS and increased permeability of bacteria in both active and dormant metabolic states.

On the basis of the effects and mechanisms observed in bacterial persister cells after treatment with Ag⁺, we hypothesized that Ag⁺ also may potentiate antibiotic activity against bacterial persister cells. We treated *E. coli* persister cells with sublethal concentrations of Ag⁺ (30 μM) and three different antibiotics (ampicillin at 10 μg/ml, ofloxacin at 3 μg/ml, and gentamicin at 5 μg/ml) individually and in combination, and observed that the combination treatments exhibited greater bactericidal activity relative to the individual treatments with Ag⁺ or each of the antibiotics (Fig. 8, D to F). Using the Bliss Model, we determined that the antimicrobial effects were synergistic between Ag⁺ and the individual antibiotics tested (fig. S15). Together, these results indicate that the multifaceted bactericidal mode of action of silver can be harnessed to enable antibiotics to kill bacterial persister cells.

Biofilms, implicated in chronic infections of the urinary tract, lungs, skin, and other areas of the body, represent a clinical challenge due to difficulties in treating them (50). We explored the possibility of using the Ag⁺-gentamicin combinatorial therapy to treat biofilms

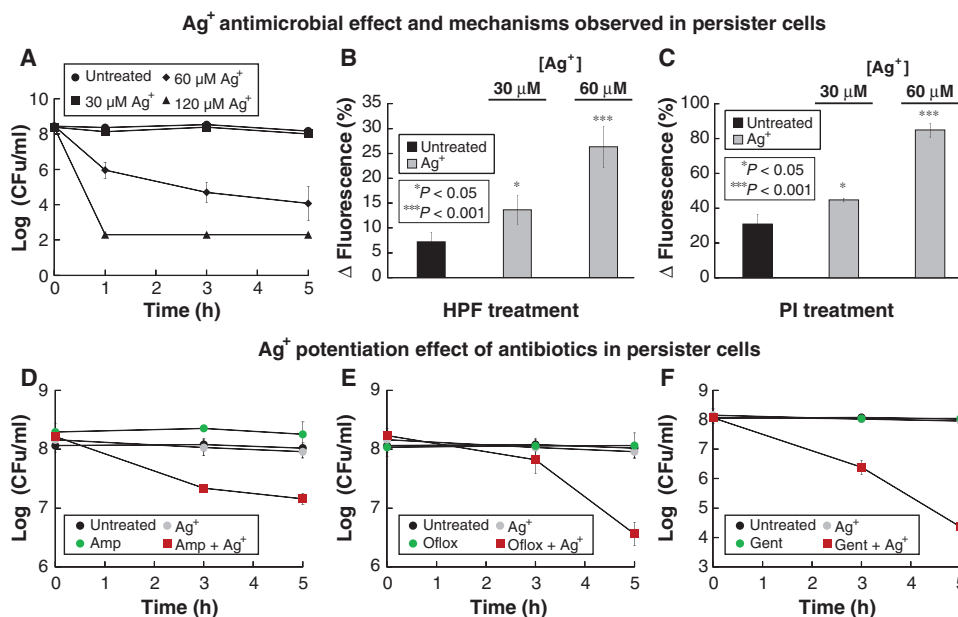


Fig. 8. Ag⁺ potentiates bactericidal antibiotic activity in vitro against bacterial persister cells. (A) Kill curves for persister *E. coli* cells treated with various concentrations of AgNO₃. (B) Changes in HPF fluorescence after 3 hours of administering AgNO₃ at various concentrations ($P < 0.05$ and $P < 0.001$ for 30 and 60 μM, respectively). (C) Changes in PI fluorescence after 3 hours of administering different concentrations of AgNO₃ ($P < 0.05$ and $P < 0.001$ for 30 and 60 μM, respectively). (D to F) Kill curves for *E. coli* persister cells treated with 30 μM AgNO₃, gentamicin (Gent) (5 μg/ml), ofloxacin (Oflox) (3 μg/ml), ampicillin (Amp) (10 μg/ml), or a combination of AgNO₃ with the respective antibiotics. Error bars represent means ± SEM from at least six biological replicates. *** $P < 0.001$, * $P < 0.05$, Student's *t* test, significant difference from the untreated control, unless otherwise indicated.

grown in vitro. *E. coli* biofilms grown overnight were treated with Ag⁺ and gentamicin individually and in combination. We observed that the combination treatment resulted in greater bacterial cell death relative to the treatments with Ag⁺ or gentamicin alone (Fig. 9, A to D).

Next, we used a mouse biofilm infection model to determine whether the potentiated bactericidal effects exhibited in vitro would be observed in an in vivo setting. Biofilms were grown in catheters that were surgically implanted subcutaneously in mice. Forty-eight hours after the catheters were implanted, the mice received no treatment or intraperitoneally delivered gentamicin, Ag⁺, or gentamicin plus Ag⁺ (Fig. 9E). The catheters were surgically removed from the mice 24 hours after treatment, and the bacterial counts showed that treatment with gentamicin presented no difference compared to the untreated control, whereas treatment with Ag⁺ alone showed a slight decrease of less than 10-fold when compared to the untreated control (Fig. 9F). The combination therapy (gentamicin plus Ag⁺) reduced cell counts in the biofilms by more than 100-fold compared to the untreated control ($P < 0.001$) (Fig. 9F). These results demonstrate the capability of Ag⁺ to potentiate antibiotic activity against biofilms in in vivo settings.

DISCUSSION

By conducting phenotypic and genetic analyses both in vitro and in vivo, we show that Ag⁺, an ancient antibacterial agent, disrupts multiple bacterial cellular networks and processes, resulting in the destabiliza-

tion of the cellular envelope and the production of ROS in Gram-negative bacteria. Our work suggests that this multitargeted antimicrobial mechanism of action is the result of silver's thiophilic chemical properties. Through exploitation of these mechanistic effects, we demonstrate that Ag⁺ can potentiate the activity of a broad range of antibiotics against Gram-negative bacteria in distinct metabolic states, establishing it as a potent antibiotic adjuvant.

Multidrug-resistant, Gram-negative bacteria are an important cause of nosocomial infections. Our data show that Ag⁺ has an antimicrobial synergistic effect against Gram-negative bacteria when used in combination with β-lactams, aminoglycosides, and quinolones. Furthermore, our work indicates that combination therapies involving Ag⁺ and large antibiotics such as vancomycin may be an option for treating Gram-negative infections. More generally, the ability of Ag⁺ to permeabilize the outer membranes of Gram-negative bacteria may enable repurposing of existing drugs to enhance the current antibiotic arsenal.

Here, we studied the effects of silver at inhibitory and lethal concentrations. We show using TEM that even at sublethal Ag⁺ concentrations, we can observe moderate morphological changes in the bacterial membrane and protein aggregates. Additionally, we demonstrate that the main phenotypes—increases in ROS production and membrane permeability—are triggered at both inhibitory and lethal silver concentrations. Further, we show that the moderate increases in membrane permeability and ROS production caused by sublethal concentrations of silver can be used to enhance the activity of antibiotics and broaden the spectrum of vancomycin. We hypothesize that the increases in ROS production are likely an indirect effect of the interaction of silver with its targets; this is supported by our findings that mutant strains that impair the primary effects of silver exhibit diminished antibiotic susceptibility and decreased ROS production. As noted earlier, two recent papers questioned the role of the ROS in antibiotic-mediated bacterial cell death (22, 23), although these findings are still the subject of debate (51, 52). Here, we show, using multiple assays and experiments, that silver treatment leads to ROS production in bacteria and that this effect can be harnessed to enhance the killing efficacy of bactericidal antibiotics in vitro and in vivo.

Even though Ag⁺ interacts with the microbial cell at multiple sites, resistance has been observed in some cases (53, 54) mainly through overexpression of copper-related efflux pumps. However, because antibacterial combination therapies involving low doses of Ag⁺ would induce cell death through the attack of multiple cellular sites, such approaches could potentially delay the emergence of resistance (55–57).

The synergistic effect between Ag⁺ and the different antibiotics is achieved when adding 15 and 30 μM Ag⁺ for metabolically active and nonactive cells, respectively. These Ag⁺ concentrations correspond to a twofold decrease when compared to the active concentration of Ag⁺

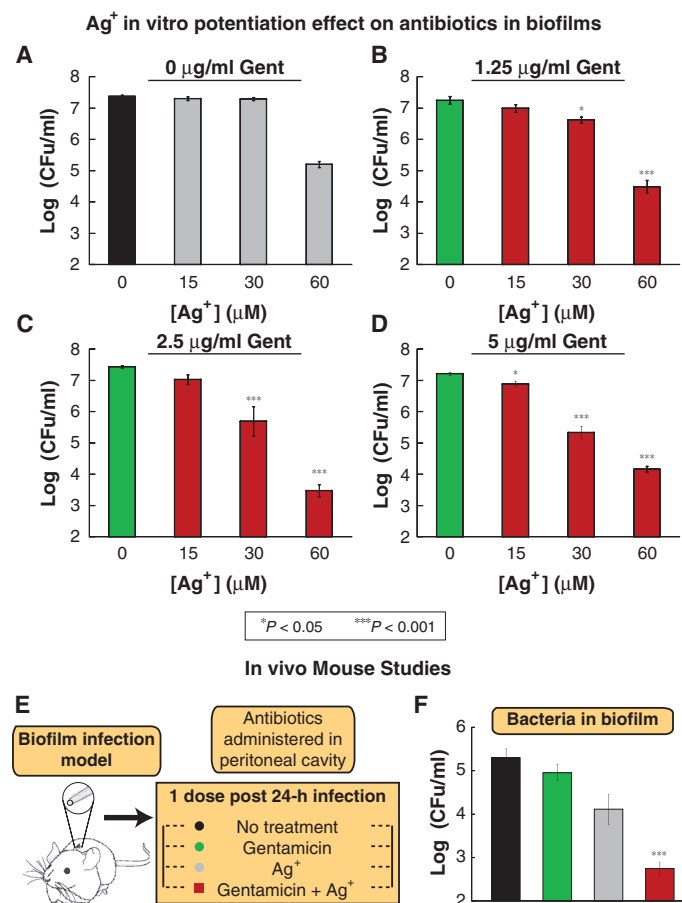


Fig. 9. Ag⁺ potentiates the bactericidal antibiotics against biofilm-producing bacteria in vitro and in vivo. (A to D) Log (CFU/ml) of *E. coli* within biofilms after treatment for 5 hours with combinations of various AgNO₃ concentrations and gentamicin (Gent) [0 (A), 1.25 (B), 2.5 (C), and 5 $\mu\text{g/ml}$ (D)]. (E) Schematic of the in vivo biofilm infection model. (F) CFU of WT *E. coli* found in the disrupted biofilm from the catheter 24 hours after no treatment or treatment with gentamicin (2.5 mg/kg), AgNO₃ (6 mg/kg) (35 μM), or gentamicin (2.5 mg/kg) in combination with AgNO₃ (6 mg/kg). Error bars represent means \pm SEM from at least six biological replicates. *** $P < 0.001$, * $P < 0.05$, Student's *t* test, significant difference from the untreated control, unless otherwise indicated.

required to treat in the absence of antibiotics. This suggests that those concentrations of Ag⁺ are necessary to trigger enough membrane permeability and/or ROS production to synergize with the antibiotics. Notably, Ag⁺ has been used successfully in topical therapeutic ointments. Moreover, our results describing the capability of Ag⁺ to enhance antibiotic activity across a wide range of antibiotics, in combination with the toxicity data, invite a future study of its use as an antibiotic adjuvant that can be orally taken or injected and used in a wider clinical setting. We are optimistic that future work from the fields of drug delivery and bionanotechnology will use new compounds containing Ag⁺ to develop more efficient and sophisticated therapies. Such could be the case for Ag⁺ in its nanoparticle form (7), which has been shown to be a more effective antimicrobial agent when compared to Ag⁺ alone. Moreover, given recent advances in nanotechnology and surface chemistry, we can envision synthesizing Ag⁺ nanoparticles with

antibiotic-decorated surfaces within an intelligent material that controls release of active antimicrobial compounds at the site of infection.

MATERIALS AND METHODS

In vitro studies

For all experiments performed with cells in exponential phase, *E. coli* overnight cultures were diluted 1:250 in 25 ml of Luria-Bertani (LB) medium and grown to an $A_{600\text{nm}}$ (absorbance at 600 nm) of 0.3 in 250-ml flasks at 37°C, 300 rpm, and 80% humidity. All antimicrobial treatments were performed in 500 μl of samples in 24-well plates incubated at 37°C, 900 rpm, and 80% humidity. For experiments with bacterial persister cells, *E. coli* were grown to stationary phase for 16 hours at 37°C, 300 rpm, and 80% humidity in 25 ml of LB. Cells were then treated with ofloxacin (5 $\mu\text{g/ml}$) for 4 hours to kill nonpersister cells. The samples were then washed with PBS and suspended in M9 minimal medium and treated with the different antibiotics to determine killing of persisters. For experiments with biofilms, an *E. coli* culture grown overnight was diluted 1:200 into MBEC Physiology and Genetic Assay wells (MBEC BioProducts) and grown for 24 hours at 30°C, 0 rpm, and 80% humidity. All wells containing biofilms were then treated with the different antibiotics. After treatment, the wells were washed with PBS three times and then sonicated for 45 min to disrupt the biofilm and plate cells to count CFU. Unless otherwise specified, the following concentrations were used in the *E. coli* antimicrobial treatments: silver nitrate, 10, 20, 30, 60, and 120 μM ; gentamicin, 0.25 and 5 $\mu\text{g/ml}$; ampicillin, 1 and 10 $\mu\text{g/ml}$; ofloxacin, 0.03 and 3 $\mu\text{g/ml}$; and vancomycin, 30 $\mu\text{g/ml}$. Kill curves for the antimicrobial treatments were obtained by spot-plating serially diluted samples and counting CFU. Gene knockout strains were constructed by P1 phage transduction from the Keio knockout mutant collection. Raw data (CFU/ml) for killing assays for all strains are given in table S2. Construction of the genetic reporter strains for iron misregulation, superoxide production, and disulfide bond formation, as well as the *sodA* overexpression strain, was performed with conventional molecular cloning techniques. The fluorescent reporter dye HPF was used as previously described (17) at 5 mM to detect hydroxyl radical (OH \bullet) formation. The fluorescent dye PI was used at concentrations of 1 mM to monitor membrane permeability. Fluorescence data were collected with a Becton Dickinson FACSCalibur flow cytometer. For the permeability and OH \bullet production assays, fluorescence of the respective dyes was determined as a percent change with the following formula: $[(\text{Fluorescence}_{\text{dye}} - \text{Fluorescence}_{\text{no dye}})/(\text{Fluorescence}_{\text{no dye}})] \times 100$. For the OH \bullet quenching experiments, cells were treated with 150 mM thiourea and AgNO₃ simultaneously. Release of protein-bound iron in an *E. coli* cell lysate was detected by incubating samples for 1 hour in a 10 mM Ferene-S assay and measuring absorbance at 593 nm. The lysates were prepared by sonication in 20 mM tris-HCl (pH 7.2) buffer. The lysates were treated with either heat (90°C for 20 min) or AgNO₃ (30 μM for 1 hour). All samples analyzed with the JEOL 1200EX 80-kV TEM were fixed with glutaraldehyde, dehydrated with ethanol, embedded with spur resin, and microtomed into ~60-nm-thick sections.

In vivo studies

Median lethal dose (LD₅₀) of parenterally delivered silver in mice. Six-week-old male C57BL/6 mice (body weight, ~20 g) were used. Ten mice per group were treated with 50 μl of intraperitoneally administered

Ag⁺ at 30, 60, 120, and 240 μM with water as the vehicle. The animals were observed for 7 days. The LD₅₀ was determined by measuring the concentrations at which only 50% of the recipient mice survived.

Analysis of diverse blood metabolites to determine mouse health. Six-week-old male C57BL/6 mice (body weight, ~20 g) were used. Three mice per group were treated with parenterally administered PBS, vancomycin (30 mg/kg), AgNO₃ (6 mg/kg) (35 μM), and vancomycin (30 mg/kg) in combination with AgNO₃ (6 mg/kg). The animals were observed for 2 days, and retro-orbital blood sample collection was performed 6, 24, and 48 hours after treatment. Blood was collected in heparinized whole-blood test tubes and further analyzed with the Piccolo Comprehensive Metabolic Reagent Disks in a Piccolo Blood Chemistry Analyzer (Abaxis).

Minimum lethal dose of *E. coli* for peritonitis mouse model. For all animal experiments, 6-week-old male C57BL/6 mice (body weight, ~20 g) were used. Serial dilutions of *E. coli* ranging from 1 × 10⁶ to 1 × 10⁹ CFU per mouse were introduced into the peritoneal cavity of the mice in 500-μl aliquots of sterile saline supplemented with 8% mucin. The animals were observed for 7 days. The minimum lethal dose (MLD) was determined to be 5 × 10⁶ CFU per mouse by measuring the lowest concentration of *E. coli* that killed 100% of the recipient mice.

Mouse peritonitis model. Inbred, wild-type male C57BL/6 mice (6 weeks; ~20 g) were used. After 1 week of quarantine, inoculation was performed by intraperitoneal injection of 500 μl of either the MLD *E. coli* inoculums (acute peritonitis model) or 1 × 10⁴ *E. coli* cells (mild peritonitis model) with a 26-gauge syringe. The inoculum was delivered in suspension with 8% (w/v) mucin in sterile saline. Either 1 hour (acute infection model) or 24 hours (mild infection model) after introduction of the inoculum, the untreated control group (*t* = 0) was euthanized and the antibacterial therapy was initiated by intraperitoneal injection of 50 μl of aliquots for the rest of the groups. Ten mice per group received antibacterial treatments. At time 0 (control only), 8, 16, and 24 hours, mice were euthanized. Peritoneal washes were performed by injecting 1.0 ml of sterile saline in the intraperitoneal cavity followed by a massage of the abdomen. Subsequently, the abdomen was opened and 200 μl of peritoneal fluid (PF) was recovered from the peritoneum for analysis of *E. coli* CFU/ml. For the CFU/ml measurement, the PF was serially diluted in PBS (pH 7.2). A 5-μl portion of each dilution was plated in LB agar plates and incubated overnight at 37°C. Colonies were counted, and CFU/ml was calculated with the following formula: [(number of colonies) × (dilution factor)]/(amount plated).

Survival assays. Six-week-old male C57BL/6 mice (weighing ~20 g) received intraperitoneal injections of the MLD of *E. coli* in a volume of 500 μl with 8% mucin. After 1 hour, 10 mice per group received 50-μl intraperitoneal injections of either vehicle (PBS) only or the different antibacterial treatments. The mice were observed for 5 days to evaluate survival.

UTI mouse model. Six-week-old female C57BL/6 mice were inoculated with 50 μl of 8% (w/v) mucin solution in sterile saline containing 2 × 10⁹ *E. coli* (MG1655) cells via transurethral catheterization into their bladders, as previously described. Briefly, mice were anesthetized with 2 to 4% isoflurane. Urinary catheters (30-gauge × 1/2-inch hypodermic needle aseptically covered with polyethylene tubing) were coated in medical-grade sterile lubricating jelly. The bladder of the mouse was gently massaged to expel urine. The lubricated catheter was inserted into the urethral opening. It was then pushed into the

urethra until the base of the needle reached the urethral opening. Once fully inserted, 50 μl of the inoculum (containing 2 × 10⁹ *E. coli* cells) was injected directly into the bladder.

Infected animals received designated drug treatments or vehicle (PBS) only via intraperitoneal delivery 24 hours after inoculation. After treatment, animals were observed for an additional 24 hours. At the end of the experiment, animals were euthanized by CO₂ asphyxiation followed by cervical dislocation. Bladders were collected in 1 ml of PBS and homogenized for 30 s for subsequent quantification of bacterial load. For the CFU/bladder measurements, the homogenized bladder was serially diluted in PBS (pH 7.2). A 200-μl portion of each dilution was plated in LB agar plates and incubated overnight at 37°C. The colonies were counted, and CFU/bladder was calculated with the following formula: {(number of colonies) × (dilution factor)}/(amount plated) × 5.

Mouse biofilm infection model. Briefly, intramedic polyethylene tubing (PE10, BD Biosciences) measuring 1 cm in length was incubated in *E. coli* cultures for 24 hours to form biofilms. The biofilm-coated tubing was surgically implanted subcutaneously on the back of 8-week-old female C57BL/6 mice under 2 to 4% isoflurane. Forty-eight hours after surgery, infected animals received designated drug treatments or vehicle (PBS) only via intraperitoneal delivery. After treatment, animals were observed for an additional 24 hours. At the end of the experiment, animals were euthanized by CO₂ asphyxiation followed by cervical dislocation. The catheter tubing was surgically removed and collected in 1 ml of PBS. The biofilm on the tubing was disrupted through sonication for 45 min for subsequent quantification of bacterial load. For the CFU/catheter measurements, the PBS was serially diluted in PBS (pH 7.2). A 200-ml portion of each dilution was plated in LB agar plates and incubated overnight at 37°C. The colonies were counted, and CFU/catheter was calculated with the following formula: {(number of colonies) × (dilution factor)}/(amount plated) × 5.

SUPPLEMENTARY MATERIALS

www.sciencetranslationalmedicine.org/cgi/content/full/5/190/190ra81/DC1

Materials and Methods

Results

References

- Fig. S1. Scavenging OH• within the cell during antibiotic treatment inhibits cell death.
 Fig. S2. Direct interaction between Ag⁺ and Fe-S clusters leads to iron misregulation, leaking of Fe²⁺, and overproduction of OH• radicals.
 Fig. S3. Ag⁺ induces activation of *soxS*, indicating production of ROS.
 Fig. S4. Ag⁺ induces moderate morphological changes and protein aggregate formation when delivered at sublethal concentrations.
 Fig. S5. PI fluorescence emitted by cells treated with a sublethal concentration of Ag⁺.
 Fig. S6. Schematic of the disulfide bond reporter construct.
 Fig. S7. Impairment of disulfide bond formation leads to increased permeability of the cellular outer membrane.
 Fig. S8. Addition of sublethal concentrations of Ag⁺ potentiates bactericidal antibiotics.
 Fig. S9. The Bliss Model for Synergy confirms a synergistic effect, between Ag⁺ and three different families of bactericidal antibiotics, against Gram-negative bacteria.
 Fig. S10. Addition of Ag⁺ broadens the spectrum of vancomycin.
 Fig. S11. The Bliss Model for Synergy confirms a synergistic effect, between Ag⁺ and vancomycin, against Gram-negative bacteria.
 Fig. S12. Reference upper level of normal (ULN) levels for mice when using the Piccolo Metabolic Disk from Abaxis.
 Fig. S13. Blood chemistry analysis of murine peripheral blood after Ag⁺ and antibiotic treatments.
 Fig. S14. Blood chemistry analysis showing that liver function enzymes detected in peripheral blood soon recover to normal levels after treatment with Ag⁺, vancomycin, and Ag⁺ plus vancomycin.
 Fig. S15. The Bliss Model for Synergy confirms a synergistic effect, between Ag⁺ and three different families of bactericidal antibiotics, against persister Gram-negative bacteria.

Table S1. MICs for different antibiotics for the MG1655 *E. coli* strain used in this study.

Table S2. Raw data showing antimicrobial effects of Ag⁺ observed in different mutants.

Table S3. Raw data showing potentiation of antibiotics using Ag⁺ as an adjuvant compound.

Table S4. MICs for different antibiotics and different *E. coli* strains used in this study.

Table S5. Raw data showing potentiation of vancomycin using Ag⁺ as an adjuvant compound.

REFERENCES AND NOTES

- G. Taubes, The bacteria fight back. *Science* **321**, 356–361 (2008).
- J. Li, R. L. Nation, J. D. Turnidge, R. W. Milne, K. Coulthard, C. R. Rayner, D. L. Paterson, Colistin: The re-emerging antibiotic for multidrug-resistant Gram-negative bacterial infections. *Lancet Infect. Dis.* **6**, 589–601 (2006).
- J. M. Pagés, C. E. James, M. Winterhalter, The porin and the permeating antibiotic: A selective diffusion barrier in Gram-negative bacteria. *Nat. Rev. Microbiol.* **6**, 893–903 (2008).
- M. E. Falagas, S. K. Kasiakou, Colistin: The revival of polymyxins for the management of multidrug-resistant Gram-negative bacterial infections. *Clin. Infect. Dis.* **40**, 1333–1341 (2005).
- S. K. Kasiakou, A. Michalopoulos, E. S. Soteriades, G. Samonis, G. J. Sermades, M. E. Falagas, Combination therapy with intravenous colistin for management of infections due to multidrug-resistant Gram-negative bacteria in patients without cystic fibrosis. *Antimicrob. Agents Chemother.* **49**, 3136–3146 (2005).
- L. N. Magner, *Hippocrates and the Hippocratic Tradition. A History of Medicine*, J. Duffy, Ed. (Marcel Dekker Inc., New York, 1992).
- J. R. Morones, J. L. Elechiguerra, A. Camacho, K. Holt, J. B. Kouri, J. T. Ramirez, M. J. Yacaman, The bactericidal effect of silver nanoparticles. *Nanotechnology* **16**, 2346–2353 (2005).
- R. B. Thurman, C. P. Gerba, G. Bitton, The molecular mechanisms of copper and silver ion disinfection of bacteria and viruses. *Crit. Rev. Environ. Control* **18**, 295–315 (1989).
- Q. L. Feng, J. Wu, G. Q. Chen, F. Z. Cui, T. N. Kim, J. O. Kim, A mechanistic study of the antibacterial effect of silver ions on *Escherichia coli* and *Staphylococcus aureus*. *J. Biomed. Mater. Res.* **52**, 662–668 (2000).
- W. K. Jung, H. C. Koo, K. W. Kim, S. H. Shin, S. H. Kim, Y. H. Park, Antibacterial activity and mechanism of action of the silver ion in *Staphylococcus aureus* and *Escherichia coli*. *Appl. Environ. Microbiol.* **74**, 2171–2178 (2008).
- R. M. Slawson, H. Lee, J. T. Trevors, Bacterial interactions with silver. *Biol. Met.* **3**, 151–154 (1990).
- K. B. Holt, A. J. Bard, Interaction of silver(I) ions with the respiratory chain of *Escherichia coli*: An electrochemical and scanning electrochemical microscopy study of the antimicrobial mechanism of micromolar Ag⁺. *Biochemistry* **44**, 13214–13223 (2005).
- H. J. Park, J. Y. Kim, J. Kim, J. H. Lee, J. S. Hahn, M. B. Gu, J. Yoon, Silver-ion-mediated reactive oxygen species generation affecting bactericidal activity. *Water Res.* **43**, 1027–1032 (2009).
- O. Gordon, T. Vig Slenbers, P. S. Brunetto, A. E. Villaruz, D. E. Sturdevant, M. Otto, R. Landmann, K. M. Fromm, Silver coordination polymers for prevention of implant infection: Thiol interaction, impact on respiratory chain enzymes, and hydroxyl radical induction. *Antimicrob. Agents Chemother.* **54**, 4208–4218 (2010).
- C. P. Randall, L. B. Oyama, J. M. Bostock, I. Chopra, A. J. O'Neill, The silver cation (Ag⁺): Antistaphylococcal activity, mode of action and resistance studies. *J. Antimicrob. Chemother.* **68**, 131–138 (2013).
- M. A. Kohanski, D. J. Dwyer, J. J. Collins, How antibiotics kill bacteria: From targets to networks. *Nat. Rev. Microbiol.* **8**, 423–435 (2010).
- M. A. Kohanski, D. J. Dwyer, B. Hayete, C. A. Lawrence, J. J. Collins, A common mechanism of cellular death induced by bactericidal antibiotics. *Cell* **130**, 797–810 (2007).
- D. J. Dwyer, D. M. Camacho, M. A. Kohanski, J. M. Callura, J. J. Collins, Antibiotic-induced bacterial cell death exhibits physiological and biochemical hallmarks of apoptosis. *Mol. Cell* **46**, 561–572 (2012).
- J. J. Foti, B. Devadoss, J. A. Winkler, J. J. Collins, G. C. Walker, Oxidation of the guanine nucleotide pool underlies cell death by bactericidal antibiotics. *Science* **336**, 315–319 (2012).
- M. A. Kohanski, D. J. Dwyer, J. Wierzbowski, G. Cottarel, J. J. Collins, Mistranslation of membrane proteins and two-component system activation trigger antibiotic-mediated cell death. *Cell* **135**, 679–690 (2008).
- D. J. Dwyer, M. A. Kohanski, B. Hayete, J. J. Collins, Gyrase inhibitors induce an oxidative damage cellular death pathway in *Escherichia coli*. *Mol. Syst. Biol.* **3**, 91 (2007).
- Y. Liu, J. A. Imlay, Cell death from antibiotics without the involvement of reactive oxygen species. *Science* **339**, 1210–1213 (2013).
- I. Keren, Y. Wu, J. Inocencio, L. R. Mulcahy, K. Lewis, Killing by bactericidal antibiotics does not depend on reactive oxygen species. *Science* **339**, 1213–1216 (2013).
- K. Setsukinai, Y. Urano, K. Kakinuma, H. J. Majima, T. Nagano, Development of novel fluorescence probes that can reliably detect reactive oxygen species and distinguish specific species. *J. Biol. Chem.* **278**, 3170–3175 (2003).
- A. Novogrodsky, A. Ravid, A. L. Rubin, K. H. Stenzel, Hydroxyl radical scavengers inhibit lymphocyte mitogenesis. *Proc. Natl. Acad. Sci. U.S.A.* **79**, 1171–1174 (1982).
- J. A. Imlay, S. M. Chin, S. Linn, Toxic DNA damage by hydrogen peroxide through the Fenton reaction in vivo and in vitro. *Science* **240**, 640–642 (1988).
- D. Touati, M. Jacques, B. Tardat, L. Bouchard, S. Despiéd, Lethal oxidative damage and mutagenesis are generated by iron in *Δfur* mutants of *Escherichia coli*: Protective role of superoxide dismutase. *J. Bacteriol.* **177**, 2305–2314 (1995).
- C. J. Schwartz, O. Djaman, J. A. Imlay, P. J. Kiley, The cysteine desulfurase, IscS, has a major role in in vivo Fe-S cluster formation in *Escherichia coli*. *Proc. Natl. Acad. Sci. U.S.A.* **97**, 9009–9014 (2000).
- F. F. Xu, J. A. Imlay, Silver(I), mercury(II), cadmium(II), and zinc(II) target exposed enzymic iron-sulfur clusters when they toxify *Escherichia coli*. *Appl. Environ. Microbiol.* **78**, 3614–3621 (2012).
- S. Chillappagari, A. Seubert, H. Trip, O. P. Kuipers, M. A. Marahel, M. Miethke, Copper stress affects iron homeostasis by destabilizing iron-sulfur cluster formation in *Bacillus subtilis*. *J. Bacteriol.* **192**, 2512–2524 (2010).
- S. Eskelinen, M. Haikonen, S. Räsänen, Ferene-S as the chromogen for serum iron determinations. *Scand. J. Clin. Lab. Invest.* **43**, 453–455 (1983).
- S. Korshunov, J. A. Imlay, Two sources of endogenous hydrogen peroxide in *Escherichia coli*. *Mol. Microbiol.* **75**, 1389–1401 (2010).
- A. Lindqvist, J. Membrillo-Hernández, R. K. Poole, G. M. Cook, Roles of respiratory oxidases in protecting *Escherichia coli* K12 from oxidative stress. *Antonie Van Leeuwenhoek* **78**, 23–31 (2000).
- S. Y. Liau, D. C. Read, W. J. Pugh, J. R. Furr, A. D. Russell, Interaction of silver nitrate with readily identifiable groups: Relationship to the antibacterial action of silver ions. *Letts. Appl. Microbiol.* **25**, 279–283 (1997).
- M. Zheng, F. Aslund, G. Storz, Activation of the OxyR transcription factor by reversible disulfide bond formation. *Science* **279**, 1718–1721 (1998).
- H. Kadokura, F. Katzen, J. Beckwith, Protein disulfide bond formation in prokaryotes. *Annu. Rev. Biochem.* **72**, 111–135 (2003).
- K. Denoncin, D. Vertommen, E. Paek, J. F. Collet, The protein-disulfide isomerase DsbC cooperates with SurA and DsbA in the assembly of the essential β -barrel protein LptD. *J. Biol. Chem.* **285**, 29425–29433 (2010).
- G. Matsumoto, H. Mori, K. Ito, Roles of SecE in ATP- and SecA-dependent protein translocation. *Proc. Natl. Acad. Sci. U.S.A.* **95**, 13567–13572 (1998).
- M. P. Brynildsen, J. A. Winkler, C. S. Spina, I. C. MacDonald, J. J. Collins, Potentiating antibacterial activity by predictably enhancing endogenous microbial ROS production. *Nat. Biotechnol.* **31**, 160–165 (2013).
- M. Hegreness, N. Shores, D. Damian, D. Hartl, R. Kishony, Accelerated evolution of resistance in multidrug environments. *Proc. Natl. Acad. Sci. U.S.A.* **105**, 13977–13981 (2008).
- M. N. Alekshun, S. B. Levy, Characterization of MarR superrepressor mutants. *J. Bacteriol.* **181**, 3303–3306 (1999).
- FDA, <http://www.accessdata.fda.gov/scripts/cder/drugsatfda>.
- J. Dequid, P. Vasseur, J. Gromez-Potentier, Experimental toxicological study of some silver derivatives. *Bull. Soc. Pharm. Lille* **1**, 23–35 (1974).
- J. S. Wold, S. A. Turnipseed, Toxicology of vancomycin in laboratory animals. *Rev. Infect. Dis.* **3** (Suppl.), S224–S229 (1981).
- S. D. Davis, Activity of gentamicin, tobramycin, polymyxin B, and colistimethate in mouse protection tests with *Pseudomonas aeruginosa*. *Antimicrob. Agents Chemother.* **8**, 50–53 (1975).
- P. B. Watkins, P. J. Seligman, J. S. Pears, M. I. Avigan, J. R. Senior, Using controlled clinical trials to learn more about acute drug-induced liver injury. *Hepatology* **48**, 1680–1689 (2008).
- C. S. Hung, K. W. Dodson, S. J. Hultgren, A murine model of urinary tract infection. *Nat. Protoc.* **4**, 1230–1243 (2009).
- K. R. Allison, M. P. Brynildsen, J. J. Collins, Metabolite-enabled eradication of bacterial persisters by aminoglycosides. *Nature* **473**, 216–220 (2011).
- N. M. Vega, K. R. Allison, A. S. Khalil, J. J. Collins, Signaling-mediated bacterial persister formation. *Nat. Chem. Biol.* **8**, 431–433 (2012).
- T. K. Lu, J. J. Collins, Dispersing biofilms with engineered enzymatic bacteriophage. *Proc. Natl. Acad. Sci. U.S.A.* **104**, 11197–11202 (2007).
- D. Hung, How antibiotics kill bacteria: New models needed? *Nat. Med.* **19**, 544–545 (2013).
- F. C. Fang, Antibiotic and ROS linkage questioned. *Nat. Biotechnol.* **31**, 415–416 (2013).
- J. García-Rivera, A. Casadevall, Melanization of *Cryptococcus neoformans* reduces its susceptibility to the antimicrobial effects of silver nitrate. *Med. Mycol.* **39**, 353–357 (2001).
- A. Gupta, K. Matsui, J. F. Lo, S. Silver, Molecular basis for resistance to silver cations in *Salmonella*. *Nat. Med.* **5**, 183–188 (1999).
- H. Kitano, A robustness-based approach to systems-oriented drug design. *Nat. Rev. Drug Discov.* **6**, 202–210 (2007).
- R. Chait, A. Craney, R. Kishony, Antibiotic interactions that select against resistance. *Nature* **446**, 668–671 (2007).

57. G. Cottarel, J. Wierzbowski, Combination drugs, an emerging option for antibacterial therapy. *Trends Biotechnol.* **25**, 547–555 (2007).

Acknowledgments: We thank the members of the Collins Lab for helpful discussions and C. Guerra for his help with some of the figure illustrations. We also thank M. Ericsson at the Harvard Medical School Cell Biology Electron Microscopy Facility, the ARCH animal facilities at Harvard Children's Hospital, and the Wyss Institute for their animal and research facilities.

Funding: Supported by the NIH Director's Pioneer Award Program and the Howard Hughes Medical Institute. **Author contributions:** All authors designed the study, analyzed results, and wrote the manuscript. J.R.M.-R. performed experiments to identify the mode of action of silver and assess its toxicity, and designed and performed animal infection model experiments and synergy studies in both metabolic states. J.A.W. aided in the design of the in vitro experiments to determine synergy between antibiotics and resensitization of resistant strains. C.S.S. aided in the design and execution of all animal infection model experiments. **Competing interests:**

Boston University has filed a patent application based on this work "Methods of treating Gram-negative microbial infections." This patent has been licensed by EnBiotix, which is a new startup focused on enhancing existing antibiotics. J.J.C. holds a minority equity stake in EnBiotix and chairs the Scientific Advisory Board of EnBiotix. The other authors declare that they have no competing interests.

Submitted 2 April 2013

Accepted 30 May 2013

Published 19 June 2013

10.1126/scitranslmed.3006276

Citation: J. R. Morones-Ramirez, J. A. Winkler, C. S. Spina, J. J. Collins, Silver enhances antibiotic activity against Gram-negative bacteria. *Sci. Transl. Med.* **5**, 190ra81 (2013).